Micro-Mechanics of Creep-Fatigue Damage in PB-SN Solder Due to Thermal Cycling—Part I: Formulation

Pradeep Sharma[1]

Abhijit Dasgupta

CALCE Electronic Products and Systems Consortium,
University of Maryland,
College Park, MD 20742

This paper presents a micro-mechanistic approach for modeling fatigue damage initiation due to cyclic creep in eutectic Pb-Sn solder. Damage mechanics due to cyclic creep is modeled with void nucleation, void growth, and void coalescence model based on micro-structural stress fields. Micro-structural stress states are estimated under viscoplastic phenomena like grain boundary sliding, its blocking at second-phase particles, and diffusional creep relaxation. In Part II of this paper, the developed creep-fatigue damage model is quantified and parametric studies are provided to better illustrate the utility of the developed model. [DOI: 10.1115/1.1493202]

1 Introduction

Eutectic Pb-Sn solder used in electronic packaging applications is known to be highly viscoplastic in use environments because of the high homologous temperatures. When used as interconnects in surface mount electronic circuit card assemblies (CCAs), these materials experience fatigue damage due to cyclic thermo-mechanical loading throughout their life cycle as well as during accelerated life tests. Quantifying the damage and relating accelerated test results to use environment are challenging tasks because of the differences in load profiles and micro-structural aging. Solder interconnects typically fail either through high strain rate fatigue (e.g., vibration) or through low strain rate creep-fatigue (e.g., thermal cycling). Micro-mechanistic models for the former have been reported by Upadhyayula [1] and Dasgupta et al. [2]. This paper reports the development of micro-mechanistic models for low strain rate cyclic creep damage in eutectic solder.

While macroscopic ''phenomenological'' damage models are attractive as design tools because of ease of implementation, they cannot be easily extrapolated to loadings or microstructures beyond the range of available data, because of their empirical nature. For more robust quantification of the damage process the underlying physical mechanisms that drive the failure process must be investigated at the micro-structural length scales. Furthermore, it is very important to base damage models explicitly on the micro-structural state because of the need to assess acceleration factors when micro-structural evolution in short accelerated test environments differ significantly from those encountered over long time scales in the life cycle environment. Furthermore, micromechanical models have the potential to be truly predictive, i.e., predict cyclic damage evolution rates based on damage behavior under monotonic loading. This capability is not possible, by definition, with empirical models. Thus the micromechanics models provide opportunity to significantly reduce cyclic durability testing.

The inter-granular damage initiation mode, typically observed in solders (as a result of creep dominated fatigue mechanism), can be accounted for by the following sequence of events: (1) continuous microcavity nucleation in the grain boundary; (2) cavity growth along the grain boundary; (3) cavity coalescence and interlinkage leading to intergranular fracture e.g. [3–10]. Mechanistic modeling of cyclic creep damage i.e., physics of nucleation, growth and coalescence of cavities all require determination of local microscale stress fields, which in turn depend on the local micro-structural features. There is a need therefore, for a model, to correlate macroscopic average stresses to local stress concentrations at heterogeneities in micro-structures similar to that of Sn-Pb solder. Henceforth this model will be referred to as a *micro-macro stress transition model*. The micro-macro transition model should include the effects of various microstructural processes prevalent under cyclic and static creep conditions: Grain boundary sliding, blocking of sliding by second-phase particles, perturbation of stress field due to presence of heterogeneities, interaction of stress fields of heterogeneities, diffusional and creep relaxation, grain coarsening, and changes in the constitutive and damage properties due to progressive damage. While there is a rich literature on computational modeling of some of these phenomena e.g., [10,11] to name a few, we develop analytical models because of the difficulty in embedding such schemes as part of the material model in large-scale structural analysis.

Very few researchers have proposed micro-mechanistic damage models for creep-fatigue interactions in solder. Wong and Helling's model based on void growth [4] uses the far-field stresses as the driving force. Local stress perturbations due to grain boundary sliding, second-phase heterogeneities, and creep relaxation are not taken into account. Their void growth model is very simplistic in nature and has ignored almost a decade of research in this area. More important, they do not consider continuous void nucleation either, although it has been shown to occur in solder [12] and it is considered to have a considerable influence on creep-fatigue durability of metals e.g., [3,10]. The micro-mechanistic model by Kuo et al. [5], also ignores nucleation and neither is their model sensitive to the local micro-structural deformation phenomena described above. Neither models use a mechanistic failure criterion. Failure is assumed to occur based on a ad-hoc geometric argument (i.e., failure occurs when void volume fraction reaches some critical level). In reality, the cavitating grain boundary fails by plastic collapse, the propensity of which is affected by progressive decrease in yield stress (due to grain coarsening and cavitation), state of damage and presence of hydrostatic stresses [13–15]. Since several local deformation and damage mechanisms are not explicitly built into the models of Wong and Helling [4] and Kuo et al. [5], deeper insights into the damage behavior of solder are difficult to obtain. For example, as shown for solder by Sharma [13,15], use of far-field stresses in some common nucleation models produces negligible void nucleation rates.

[1]Corresponding author: sharma@crd.ge.com

Contributed by the Electronic and Photonic Packaging Division for publication in the JOURNAL OF ELECTRONIC PACKAGING. Manuscript received by the EPPD December 21, 2001.

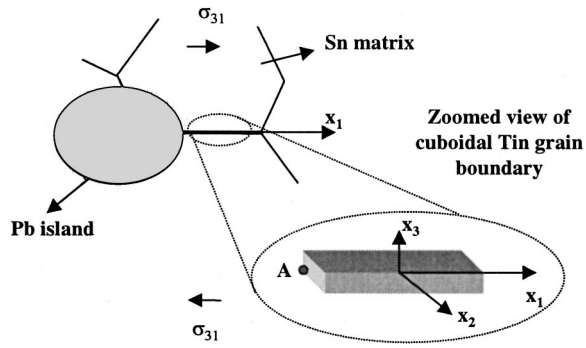

Fig. 1 Idealized geometric configuration of the physical problem

The elements of the micro-mechanics creep-fatigue damage model are explained in Sections 2–5. In Section 2, the micro-macro transition model is briefly described. In Sections 3, 4, and 5, void nucleation, void growth, and void coalescence, respectively, are discussed. Existing models are used or modified appropriately and new ones are developed, as necessary. Instantaneous grain size is an integral part of the micro-macro transition model and thus is also included in the damage formulations. In Section 6, cyclic softening is discussed. The complete creep-fatigue damage model is summarized in Section 7 and we conclude with a summary in Section 8.

2 Micro-Macro Stress Transition Model

The microstructural morphology, which needs to be modeled, is shown schematically in Fig. 1. An equiaxed Pb island is assumed to be surrounded by a polycrystalline Sn matrix. Some grain boundaries in the Sn matrix intersect with the Pb island. Grain boundaries in the tin matrix slide viscously at high temperatures and when impeded by second-phase Pb particles, generate high local stress concentrations at the particle-matrix interface. At high temperatures, creep mechanisms such as grain boundary diffusion, interfacial and volume diffusion, dislocation glide-climb, and void nucleation, tend to relax the high stress concentrations developed due to blocking of grain boundary sliding.

We have formulated the micro-macro stress analysis problem using Eshelby's formalism of eigenstrains [16]. The complete details of the micro-macro transition model are beyond the scope of the present paper and have been presented elsewhere [17]. Only an overview is presented here.

For simplicity of demonstration, the second-phase particle (Pb phase) is modeled as a spherical *inhomogeneity* (see Mura [18], for detailed definitions of inclusions, inhomogeneities and eigenstrains) situated at the end of the grain boundaries. The impinging grain boundary is modeled as a cuboidal *inclusion* with a prescribed shear *eigenstrain* (which is equal to the grain boundary sliding strain). The spherical inhomogeneity has radius "a" while the cuboidal inclusion has half-lengths a_1, a_2, and a_3. The surrounding matrix is assumed to be isotropic and elastic.

This geometric configuration is capable of modeling a wide variety of realistic microstructures. The local stresses at point A are of primary interest because that is where the highest tensile mean stresses occur and drive void nucleation. The resulting stress field has contributions from: (i) blocking of the grain boundary sliding; and (ii) interactions with the second phase particle. Thus Eshelby's formalism is an attractive mathematical model for these physical phenomena. Details of the model are presented elsewhere [17] and only the final expression is presented here:

Ω_e: (Point A, Fig. 1)

$$\sigma_{ij} = C_{ijkl}(\varepsilon^o_{kl} + S^e_{ijkl}(\varepsilon^*_{kl} + \varepsilon^{R1}_{kl}) + D^{c\_A}_{ijkl}(\varepsilon^{gbs}_{kl} + \varepsilon^{R2}_{kl}) - \varepsilon^*_{kl})$$
$$= C^h_{ijkl}(\varepsilon^o_{kl} + S^e_{ijkl}(\varepsilon^*_{kl} + \varepsilon^{R1}_{kl}) + D^{c\_A}_{ijkl}(\varepsilon^{gbs}_{kl} + \varepsilon^{R2}_{kl})) \quad (1)$$

Definitions are included in the Nomenclature. Ω_e: $(x_i = A)$ indicates that these equations are solved in the region of the ellipsoid at point A marked in Fig. 1. ε^* is nonuniform due to the interaction of grain boundary stress field and the inhomogeneity [19] and thus (1) represents a set of 6 coupled singular integral equations. Researchers solve these equations typically by expanding the nonuniform eigenstrain fields into Taylor's series [19,20]. However, as shown by Rodin and Hwang [20], convergence is very slow when the inclusions are almost touching each other and accurate analytical formulation is all but impossible. As a simplifying approximation, for ease of computation, we evaluate Eqs. (1) at point A (Fig. 1) and use the resulting fictitious eigenstrain as a representative uniform estimate of the average eigenstrain field. Such an approximation has been shown to represent the mechanics well when the inhomogeneities are almost touching each other and only the interfacial stress concentration is sought [13,17].

Mori et al. [21] and Onaka et al. [22] showed that when complete interfacial and long-range volume diffusional relaxation takes place, the stress state becomes uniformly hydrostatic and equal to the applied stress (i.e. the inhomogeneity acts as if it was not present). Thus the final state of $\varepsilon^{\mathbf{R1}}$ is such that the fictitious eigenstrain to model the inhomogeneity as an equivalent inclusion is nullified [16]. The grain boundary sliding strain is a shearing strain and volume diffusion does not play a role. In the case of cuboidal inclusion with shear eigenstrain, diffusion occurs along the inclusion interface (i.e., grain boundary diffusion) until the grain boundary sliding eigenstrain disappears (i.e., the inclusion ceases to exist). Since for any given eigenstrain, the resulting perturbed stress field in a cuboidal inclusion is always nonuniform [18,23], uniform hydrostatic stress state is not possible and complete relaxation can only occur when $\varepsilon^{\mathbf{R2}} + \varepsilon^{gbs} \rightarrow 0$ at $t \rightarrow \infty$. This discussion can be summarized as follows: (1) $\varepsilon^{\mathbf{R1}}(t \rightarrow \infty) = -\varepsilon^*(t \rightarrow \infty)$, (2) $\varepsilon^{\mathbf{R2}}(t \rightarrow \infty) = -\varepsilon^{gbs}(t \rightarrow \infty)$

It is necessary to compute the time dependent grain boundary sliding strain. It is well known that the grain boundary sliding strain is some fraction of the total creep strain (see, for example, Ashby [24] and Raj and Ashby [25]) for some early pioneering work in this area). This fraction must be deduced from experimental observations and is different for different materials and depends on several parameters for the same materials (e.g., temperature, strain rate).

Strain due to grain boundary sliding (assuming Newtonian viscosity) can be written as e.g. [3,26,27]:

$$\varepsilon^{gbs}_{31}(t) = -\varepsilon^{\max}_{31}(1 - e^{-t/tgbs}) \quad (2)$$

where, t_{gbs} is the characteristic time for sliding, which depends on the intrinsic grain boundary viscosity (defined in Eq. 4). $\varepsilon^{\max}$ is the maximum strain due to sliding which would have accumulated had the grain boundary been free to slide (i.e., not impeded by the particle). The linear dependence of shear stress on sliding rate, i.e.,

$$\dot{u} = \frac{\tau}{\eta} \quad (3)$$

The grain boundary viscosity is derived by Raj and Ashby [25] for a variety of grain boundary types. For "reasonably" flat grain boundary, its viscosity can be represented as [28]

$$\eta = \frac{kT}{8bD_b\delta_b} \quad (4)$$

The characteristic time for sliding can now be given as [3,27,29]

$$t_{gbs}=\frac{d\eta}{G}\phi \tag{5}$$

ϕ is an unknown dimensionless factor that is closely related to the geometrical characteristics of the grain boundary. It can only be determined through indirect means. However, Eqs. (4) and (5) are valid for all materials.

Thus, the final expression for t_{gbs} is

$$t_{gbs}=\frac{dkT}{8bD_b\delta_b G}\phi \tag{6}$$

Note that $D_b\delta_b$ follows an Arrhenius relationship in temperature i.e.,

$$D_b\delta_b=D_{bo}\delta_b \exp\left(-\frac{\Delta H}{kT}\right) \tag{7}$$

The term $\varepsilon^{\max}$, is harder to determine. The formulation in this paper will be demonstrated on Sn-Pb eutectic solder. Experiments by Lee and Stone [30] on solder show that the contribution of grain boundary sliding to the overall strain is nearly 0.25 in the entire range of strain rates within which grain boundary sliding does occur. Further, if far field stress is held constant, in the long-term limit, the far field creep strain will reach rupture strains. In this study, $\varepsilon^{\max}$ is chosen to be approximately $1/4^{\text{th}}$ of the rupture strain for the given temperature and stress. Since rupture strain also follows an Arrehenious relationship with respect to temperature and stress, the sliding eigenstrain is given by:

$$\varepsilon^{\max}=A_{gbs}\sigma^m \exp\left(-\frac{\Delta H_{gbs}}{kT}\right) \tag{8}$$

Within the inhomogeneity, relaxation proceeds with a combination of volumetric and interfacial diffusion. First, interfacial diffusion (which is the faster of the two) will relax the shear stresses such that stress state becomes hydrostatic. Note that although both interfacial and volume diffusion occur, the relaxation time t_v is taken to be that of volume diffusion as it is orders of magnitude slower than interfacial diffusion. Volumetric diffusion will ensue in such a manner as to counteract the fictitious eigenstrain until perturbations of the inhomogeneity vanish. According to Onaka et al. [22], the volumetric relaxation eigenstrain can be represented as:

$$\varepsilon_{ij}^{R1}(t)=-\varepsilon_{ij}^{*}(1-e^{-t/t_v}) \tag{9}$$

Based on the method of Onaka et al. [22], an expression for t_v can be easily derived. The final expression for a spherical particle is:

$$t_v=\frac{kTa^2(3K^h+4G)}{12GK^h\Omega D_v} \tag{10}$$

The superscript h indicates the inhomogeneity. This expression can also be easily evaluated for an ellipsoidal particle (which however would require numerical computation of elliptical integrals). A spherical inhomogeneity was chosen in this study as the volume diffusion was found to be too slow to cause any difference in the results (and thus did not warrant the extra accuracy).

The relaxation mechanism within the cuboidal inclusion is conceived as grain boundary diffusion such that the net volume of the grain boundary does not change i.e., diffusion occurs along the grain boundary to relieve the grain boundary sliding strain and also follows first order kinetics [21]:

$$\varepsilon_{31}^{R2}(t)=-\varepsilon_{31}^{\max}(1-e^{-t/tgbr}) \tag{11}$$

The derivation of t_{gbr} (characteristic diffusional relaxation time) can be derived based on two different methods. Mori et al. [21] use a mechanistic method to derive an expression for interfacial relaxation time for a spherical inhomogeneity subjected to pure shear. An alternative method is also possible [17] which results in similar relaxation equations. The final expression for t_{gbr} can be expressed as

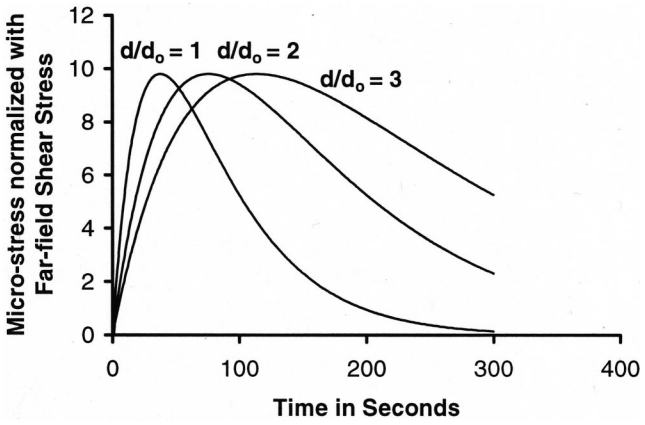

Fig. 2 Variation of normalized micro-stress with time

$$t_{gbr}=\frac{kTV_g}{G\Omega D_b\delta_b}\xi \tag{12}$$

ξ (like ϕ) is a local dimensionless geometrical factor which can only be inferred indirectly. Note that, in the micro-macro transition model, we introduce two new constants, ϕ and ξ (apart from the customary material and constitutive properties like elastic modulus, diffusion coefficient etc.) They are characteristic of the grain boundary sliding and relaxation kinetics and are related to the geometry of the grain boundary. They can best be estimated experimentally by examining the time-dependent rise and fall of stress concentrations at intersections of sliding grain boundaries and particles, perhaps through techniques such as moire interferometer (as illustrated by Han [31]). For now, these constants have been estimated approximately by inspecting relaxation data available in the literature on solder.

Sample results of the micro-stress variation is shown are Fig. 2. The results are plotted for different grain sizes. Only a far field shear stress is applied (numerical inputs can be obtained from Sharma and Dasgupta, [17]). The resulting principal normal stress at the particle-matrix interface is plotted (normalized with respect to the applied stress). As expected, stresses build up and relax with time reverting finally to the average macroscale applied stress. Thus even under an overall pure shear stress, the microstresses have tensile normal stresses due to grain anisotropy and grain boundary sliding.

3 Void Nucleation

The micro-scale stresses, estimated in Section 2, cause void nucleation by mechanisms that are not fully understood. The only thing that is certain is that void nucleation is a continuous process and the rates are indeed sensitive to local micro-scale phenomena and stress state. For the purposes of this study, a nucleation model suggested by Giessen and Tvergaard [9], is modified appropriately. Thus the nucleation rate model presented in Eq. (13) is used in conjunction with the micro-macro transition model.

$$\dot{N}=F_o\frac{N_{\max}-N}{N_{\max}}\dot{\varepsilon}_c\left(\frac{\sigma_n}{\sigma_o}\right) \quad \sigma_m>0 \tag{13}$$

Here, the stresses, strains and strain rates are to be considered local to the nucleation sites. This nucleation model requires that local σ_m (hydrostatic stress) be positive for nucleation to occur.

4 Void Growth

Void growth occurs by three main mechanisms: grain boundary diffusion, power law creep, and grain boundary sliding. Models are available in the literature for the first two mechanism and usually an upper bound solution is used for the mechanism of grain boundary sliding (see for example Onck [10]). A more realistic (mechanistic) model for grain boundary sliding induced void growth is described elsewhere by the authors [13,14] and only the final expressions are given here.

Void growth due to diffusion has been solved by several people e.g. [32,33].
The final expression is:

$$\dot{V}_{diff} = 4\pi \frac{D_b \delta_b \Omega}{kT} \frac{\sigma_b - (1-\omega)\sigma_s}{\ln(1/\omega) - (3-\omega)(1-\omega)/2} \tag{14}$$

Similarly, void growth due to power law creep can be represented by (Budiansky et al. [34], Tvergaard [35]):

$$\dot{V}_{cr} = 2\pi \dot{\varepsilon}_e R^3 h[\alpha_n + \beta_n]^n (\sigma_m/\sigma_e) \tag{15}$$

$$\dot{V}_{cr} = \mathrm{sgn}(\sigma_m) 2\pi \dot{\varepsilon}_e R^3 h[\alpha_n (\sigma_m/\sigma_e) + \beta_n]^n \tag{16}$$

Equation (15) is used for low triaxialities ($\sigma_m/\sigma_e < 1$) while Eq. (16) is used for triaxiality ratio greater than or equal to one.

The stresses, and strain rates are to be considered local to the grain boundary facet though remote from the cavity. The void growth due to grain boundary sliding can be written as [13,14]:

$$\dot{V}_{gbs} = \pi \frac{D_b \delta_b \Omega}{kT} \frac{R}{d} SE\varepsilon_{gbs} \tag{17}$$

5 Void Interlinkage

The voids grow and interlink leading eventually to a macroscale crack. A rigorous mechanistic failure criterion can be established based on the theory of cavitation instability, grain coarsening, progressive degradation of yield strength due to grain coarsening, porosity, and hydrostatic stresses [13,14]. Details are not presented here as they are quite involved and the reader is referred to Sharma and Dasgupta [14] for derivations. The input to the void interlinkage models are simply the temperature and grain size dependent yield stress, the micro-stresses, current volume fraction of voids (deduced from void growth and the average void spacing (deduced from nucleation rate).

6 Cyclic Softening and Grain Coarsening

As the void fraction continues to increase, the material continues to soften. The Mori-Tanaka [36] method for estimating average stress in the matrix and in inclusions can be used for computing the change in tangent elastic properties due to cavitation. We only present here the final expression:

$$C^{\mathrm{eff}}_{ijkl} = C^M_{klmn}\{(1-f)\Delta C_{nnpq} S_{pqrs} + C^M_{mnrs}\}^{-1} \times [\Delta C_{rstu}\{(1-f)S_{tuij} + f\delta_{tuij}\} + C^M_{rsij}] \tag{18}$$

For effective creep properties, the Mori-Tanaka method can be extended to nonlinear composites by using the method of Lin [37]. Only the final expression is retained here. The steady-state creep constitutive law for a void-free material can be expressed as

$$\dot{\varepsilon}_e = A\sigma_e^n \exp\left(-\frac{\Delta H}{kt}\right) \tag{19}$$

Here the symbols have their usual meaning. Increasing porosity changes it by altering the premultiplier in Eq. (19) as follows:

$$\dot{\varepsilon}_e = \left[\frac{1+0.67f}{(1-f)^n}\right] A\sigma_e^n \exp\left(-\frac{\Delta H}{kT}\right) \tag{20}$$

Grain coarsening affects micro-stresses, nucleation, void growth, and void linkage and thus must be taken into account. We do so by using the following grain coarsening law [1,38]

$$d^3(t) - d_0^3(t) = \frac{c_1 t}{T} \exp\left(-\frac{\Delta H_g}{RT}\right)\left[1 + \frac{\Delta\sigma}{c_2}\right] \tag{21}$$

Here, d is the current grain size, d_o is the initial grain size, c_1 and c_2 are model constants, $\Delta\sigma$ is the cyclic stress range, ΔH_g is the activation energy for the coarsening process (which is nearly equal to that of lattice or volume diffusion), R is the gas constant, T is the absolute temperature while t is time. The issue of coarsening in solders has been explored in depth by several researchers. A comprehensive review and discussion is provided by Upadhyayula [1]. Note that the grain coarsening law, as modified and used by Upadhyayula [1], is not suitable for thermo-mechanical cycling as it uses the stress range for the entire fatigue cycle and the mean temperature. Thus, for the purposes of this work, this coarsening law was used incrementally where instantaneous temperatures and stress values were used to incrementally calculate grain coarsening.

7 Creep Fatigue Damage Model

The elements described in Sections 2–6 can be combined to form a creep-fatigue damage model. The void radius fraction can be represented by

$$f_r = \frac{R}{\lambda} \tag{22}$$

As before, R is the void radius while λ is the inter-void half-spacing. The evolution of "R" occurs as per void growth Eqs. (14)–(17). The evolution of λ is seen as linked to the nucleation rate. The main effect of continuous nucleation of voids (at a finite rate) is to decrease the average intervoid spacing [10]. It can be easily deduced that:

$$\lambda = \lambda_o \sqrt{\frac{N_o}{N}} \tag{23}$$

where the subscript o indicates initial values.

The damage is defined as the ratio of the void radius fraction to critical void radius fraction required for cavitation instability. Thus, the damage can be represented by

$$D = \frac{f_r}{f_r^{crit}} \tag{24}$$

f_r^{crit} is estimated based on plastic instability theory, as discussed in Section 5. The grain size and temperature (which affect yield strength) strongly influences the determination of critical void radius fraction [13]. $D=1$ indicates complete failure. Under compression, where the critical void radius fraction is 1, the actual damage and f_r are identical.

The micro-mechanics based cyclic creep-fatigue model is implemented in an incremental-iterative manner. For a given temperature history, the global macro-scale stress analysis is carried out using any conventional technique. Since we are dealing with a creep problem, it is necessary to perform a nonlinear stress analysis. Numerical techniques such as the finite element method, can be employed or if the geometry and loading conditions are simple, semi-analytical tools can also be used. In any case, what is desired is the complete macro-scale stress history for the entire thermal cycle.

This macroscale stress history will serve as the far-field stress boundary conditions for the micro-scale model. Of course, as the material becomes damaged, the macro-scale stress-state will also change due to changes in the constitutive properties. This is fully considered in our formulation. For a complicated structure the stress-state will be non-uniform and thus each element in the finite element mesh will have a different macro-scale stress history (if

the finite element technique is used). The procedure for implementing the developed model then will have to be applied for each element. However, in this study, for illustration purposes, a simple example is chosen such that assumptions of uniform stress-state can be made. For now, it is assumed that regardless of whether the entire structure is targeted or a small element within the structure is considered, the stress history for the given thermal cycle is known.

As is done in most computational nonlinear procedures, the far-field stress history is discretized into a series of piecewise constant stress dwells and instantaneous ramps. For each constant-stress increment, we can assume the far-field stress to be held constant for a small duration of time. Under such constant far-field stress, the micro-macro transition model is applied. The time interval for which this far-field stress is held constant is further finely discretized to compute the time-dependent micro-stress state. As voids grow and interact, the stress field in the tin matrix gets perturbed and alters significantly. These stresses are not appreciably different during the early stages of damage when the void volume fraction is small, however, they contribute significantly at larger void volume fractions (> 0.15). In fact, stress disturbances due to the growing voids are primarily responsible for the acceleration of damage towards the end of the material's life.

Evolution of R and λ, and hence the damage, is deduced for each constant-stress increment. Based on the current grain size (Eq. (21)), yield stress and state-of-damage the failure surface is also computed. If damage is within the failure locus, calculations for the next increment are initiated. This process is repeated until the entire thermal cycle is modeled.

Note that the grain size is also updated incrementally along the thermal cycle. Since not much difference is expected in constitutive properties after each increment, these are only updated once per macro-cycle (i.e., at the end of each cycle). The new elastic and creep modulus is calculated based on the state of damage. Since temperature-dependent Hall-Petch constants are used, yield stress variation with both grain size and temperature is taken into account.

8 Summary

The micromechanical elements comprising various facets of cyclic creep damage were systematically combined to form a complete microstructural cyclic creep damage model. Although, there are several general aspects of this model, it is primarily tailored to the micro-structure of eutectic Sn-Pb solder. The developed model is fully capable of mechanistically taking into account local microstructural phenomena and features such as grain boundary sliding, grain size, hydrostatic stresses etc. Perhaps the most significant aspect of this model is that a rigorous mechanistic capability is now available, to predict cyclic durability based on monotonic test data. This has very significant implications in terms of resources, especially when evaluating a number of new solder candidates e.g., lead free and high temperature materials. This and other features of the developed model are explored with the help of an example and a series of parametric studies of practical interest in Part II of this paper.

Nomenclature

$\mathbf{C}$, $\mathbf{C^h}$ = fourth-order elastic stiffness tensor of solder and lead, respectively

$\boldsymbol{\varepsilon^0}, \boldsymbol{\varepsilon^*}$ = far field or global strain tensor and Fictitious eigenstrain tensor, respectively

$\mathbf{S^e}$ = Eshelby's tensor for interior points

$\mathbf{D^c}$ = Eshelby's tensor for the cuboidal shape (for exterior points)

_A = subscript indicated that the cuboidal Eshelby's tensor is evaluated at point A

$\boldsymbol{\varepsilon^{R1}}$, $\boldsymbol{\varepsilon^{R2}}$ = eigenstrains representing volume and interfacial diffusion, respectively

Ω = atomic volume

k = Boltzman's constant

d = grain size

$D_b\delta_b$ = grain boundary and thickness coefficient

S = shape factor (gbs void-growth model)

σ_n = local normal stress at particle-matrix interface

$\varepsilon_c/\varepsilon_e$ = equivalent strain or creep strain

F_o = model constant for nucleation model

σ_o = normalization constant in nucleation model

$N_{\max}$ = max number of nucleation sites per unit grain boundary area

N = instantaneous number of nucleation sites per unit grain boundary area

N_o = initial number of nucleation sites per unit grain boundary area

ϕ = shape factor used in relaxation equation

h = shape factor to calculate void volume (assuming spherical caps geometry; see Riedel [3])

ξ = shape factor used in relaxation equations

λ = intervoid half spacing

R = void radius

σ_m = local hydrostatic stress

σ_e = local equivalent stress

α_n = constant depending on creep stress exponent n

β_n = constant depending on creep stress exponent n

σ_b = average normal stress on the grain boundary; used in void growth equation due to diffusion

σ_s = sintering stress

ε^{gbs} = grain boundary sliding strain

K, K^h = bulk modulus of solder and Pb, respectively

T = temperature

t_{gbs} = characteristic time for grain boundary sliding

t_{gbd} = characteristic time for grain boundary diffusional relaxation

t_v = characteristic time for volumetric diffusional relaxation

ω = area fraction of void: $(R/\lambda)^2$

η = grain boundary viscosity

V_g = volume of the grain boundary

R_g = gas constant

a = Pb particle radius

D_v = coefficient of volume diffusion

b = atomic diameter

References

[1] Upadhyayula, K. S., 1998, Ph.D. Dissertation, Dept. of Mechanical Engineering, University of Maryland, College Park.

[2] Dasgupta, A., Sharma, P., and Upadhyayula, K., 2001, International Journal of Damage Mechanics, **10**(2), pp. 101–132.

[3] Riedel, H., 1987, *Fracture at High Temperature*, Springer-Verlag, Heidelberg, Germany.

[4] Wong, B., and Helling, D. E., 1990, ASME J. Electron. Packag., **112**, pp. 104–109.

[5] Kuo, C. G., Sastry, S. M. L., and Jerina, K. L., 1995, Metall. Mater. Trans. A, **26A**, pp. 3625–3275.

[6] Raj, R., and Ashby, M. F., 1975, Acta Metall., **23**, pp. 653–666.

[7] Cocks, A. C. F., and Ashby, M. F., 1982, "On Creep Fracture by Void Growth," Prog. Mater. Sci., **27**, pp. 189–244.

[8] Needleman, A., and Rice, J. R., Acta Metall., **28**, pp. 1315–1332.

[9] Giessen, E. V. D. and Tvergaard, V., 1990, *Creep and Fracture of Engineering Materials and Structures*, Wilshire, B. and Evans, R. W., ed., Elsevier, Swansea, pp. 169–178.

[10] Onck, P. R., 1998. *High Temperature Fracture of Polycrystalline Materials*, PhD thesis, Technical University Delft, Netherlands.

[11] Giessen, E. V. D., and Tvergaard, V., 1996, Acta Metall., **44**, pp. 2697–2710.

[12] Lee, S. M., 1995, Japanese Journal of Applied Physics, Part 2 (Letters), **34**(11A), pp. L1475–7.

[13] Sharma, P., 2000, Ph.D. dissertation, Dept. of Mechanical Engineering, University of Maryland, College Park.

[14] Sharma, P., and Dasgupta, A., 2001, subitted to ASME J. Eng. Mater. Technol.

[15] Dasgupta, A., Sharma, P., and Upadhyayula, K., 2001, "Micro-Mechanics of

Fatigue Damage in Pb-Sn Solder. Due to Vibration and Thermal Cycling,'' Int. J. Damage Mech., **10**(2), pp. 101–132.
[16] Eshelby, J. D., 1957, Proc. R. Soc. London, Ser. A, **A241**, pp. 376–396.
[17] Sharma, P., and Dasgupta, A., submitted to the Journal of Applied Physics.
[18] Mura, T., 1987, *Micromechanics of Defects in Solids*, Martinus Nijhoff, Hague, Netherlands.
[19] Moshcovidis, Z. A., and Mura, T., 1975, ASME J. Appl. Mech., **42**, pp. 847–852.
[20] Rodin, G. J., and Hwang, Y. L., 1991, Int. J. Solids Struct., **27**, pp. 145–159.
[21] Mori, T., Okabe, M., and Mura, T., 1980, Acta Metall., **28**, pp. 319–325.
[22] Onaka, S., Miura, S., and Kato, M., 1990, Mechanics of Materials., **8**, pp. 285–292.
[23] Chiu, Y. P., 1977, ASME J. Appl. Mech., **44**, pp. 587–590.
[24] Ashby, M. F., 1972, ''Boundary Defects and Atomistic Aspects of Boundary Sliding and Diffusional Creep,'' Surf. Sci., **31**(1), pp. 498–542.
[25] Raj, R., and Ashby, M. F., 1971, Metallurgical Transactions, **2**, pp. 113–1127.
[26] Tanaka, M., and Iizuka, H., 1988, ''A Micromechanics Model of the Initiation of Grain Boundary Crack in High Temperature Fatigue,'' Low Cycle Fatigue, ASTM STP 942, H. D. Solomon, G. R., Halford, L. R., Kaisand, and B. N., Leis, eds., ASTM, Philadelphia, pp. 611–621.
[27] Chan, K. S., Page, R. A., Lankford, J., 1986, Acta Metall., **34**, pp. 2361–2370.
[28] Crossman, F. W., and Ashby, M. F., 1975, Acta Metall., **23**, pp. 425–440.
[29] Argon, A. S., Chen, I. W., and Lau, C. W., 1980 ''Intergranular Cavitation in Creep: Theory and Experiments,'' *Creep-Fatigue-Environment Interaction*, Pelloux, R. M. and Stoloff, N. S., Eds.
[30] Lee, S. M., and Stone, D. S., 1994, Scr. Metall., **30**, pp. 1213–1218.
[31] Han, B., 1996, Exp. Mech., June, pp. 120–126.
[32] Hull, D., and Rimmer, D. E., 1959, Philos. Mag., **4**, pp. 673–687.
[33] Rice, J. R., 1980, ''Three Dimensional Constitutive Relations and Ductile Fracture,'' *Proceedings of the IUTAM symposium*, Nemat-Nasser, ed., pp. 173–184.
[34] Budiansky, B., Hutchinson, J. W., Slutsky, S., 1982, ''Void Growth and Collapse in Viscous Solids,'' H. G. Hopkins, M. J Sewell eds., *Mechanics of Solids*, The Rodney Hill 60th Anniversary Volume, Pergamon Press, Oxford.
[35] Tvergaard, V., 1984, ''On the Creep Constrained Diffusive Cavitation of Grain Boundary Facets,'' J. Mech. Phys. Solids, **32**, pp. 373–393.
[36] Mori, T., and Tanaka, K., 1973, ''Average Stress in Matrix and Average Elastic Energy of Materials with Misfitting Inclusions,'' Acta Metall., **21**(5), pp. 571–574.
[37] Lin, S. C., 1994, ''The Equivalent Inclusion Method in Elasticity and Composite Materials,'' PhD dissertation submitted to Northwestern University, Ill.
[38] Hacke, P. L., Sprecher, A. F., and Conrad, H., 1997, ''Microstructure Coarsening During Thermomechanical Fatigue of Pb-Sn Solder Joints,'' J. Electron. Mater., **26**, pp. 774–782.